ACS APPLIED MATERIALS & INTERFACES

Research Article

Cite This: ACS Appl. Mater. Interfaces 2020, 12, 1698−1706

www.acsami.org

Synergetic Effect of Porous Elastomer and Percolation of Carbon Nanotube Filler toward High Performance Capacitive Pressure Sensors

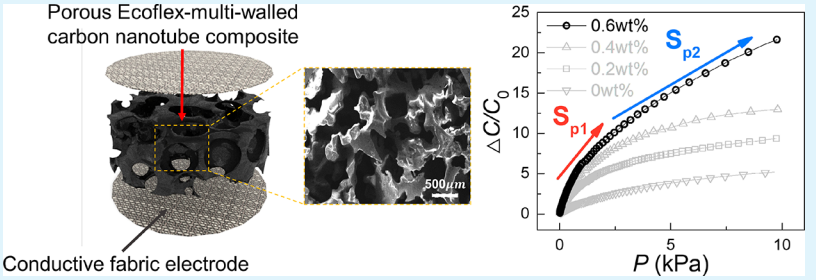
Jungrak Choi,[†] Donguk Kwon,[‡] Kyuyoung Kim,[†] Jaeho Park,[†] Dionisio Del Orbe,[†] Jimin Gu,[†] Junseong Ahn,[†] Incheol Cho,[†] Yongrok Jeong,[†] Yongsuk Oh,*[,§] and Inkyu Park*[,†]

[†]Department of Mechanical Engineering, Korea Advanced Institute of Science and Technology (KAIST), 291 Daehak-ro, Yuseong-gu, Daejeon 305-701, South Korea

[‡]Package Process Development Team, Samsung Electronics, Seoul, South Korea

[§]Center for Bio-Integrated Electronics (CBIE), Northwestern University, Evanston, Illinois 60208, United States

Supporting Information



ABSTRACT: Wearable pressure sensors have been attracting great attention for a variety of practical applications, including electronic skin, smart textiles, and healthcare devices. However, it is still challenging to realize wearable pressure sensors with sufficient sensitivity and low hysteresis under small mechanical stimuli. Herein, we introduce simple, cost-effective, and sensitive capacitive pressure sensor based on porous Ecoflex-multiwalled carbon nanotube composite (PEMC) structures, which leads to enhancing the sensitivity (6.42 and 1.72 kPa^{-1} in a range of 0−2 and 2−10 kPa, respectively) due to a synergetic effect of the porous elastomer and percolation of carbon nanotube fillers. The PEMC structure shows excellent mechanical deformability and compliance for an effective integration with practical wearable devices. Also, the PEMC-based pressure sensor shows not only the long-term stability, low-hysteresis, and fast response under dynamic loading but also the high robustness against temperature and humidity changes. Finally, we demonstrate a prosthetic robot finger integrated with a PEMC-based pressure sensor and an actuator as well as a healthcare wristband capable of continuously monitoring blood pressure and heart rate.

KEYWORDS: *wearable sensor, capacitive pressure sensor, carbon nanotube, microporous elastomer, healthcare monitoring, human−robot interface*

INTRODUCTION

Wearable pressure sensors have attracted significant interest due to their great potential in a variety of applications, including healthcare monitoring,[1−4] human−machine interfaces,[5−7] and electronic textiles.[8−10] Especially, wearable pressure sensors capable of detecting a low-pressure regime (~10 kPa, comparable to gentle touch) and a medium-pressure regime (10−100 kPa, suitable for object manipulation) are essentially required for use in wearable applications. However, there are still challenges in accurate detection of subtle pressure with sufficient sensitivity and low hysteresis, which require the rational design of promising materials and devices.

In general, the wearable pressure sensor has been constructed based on various principles, namely, resistive,[11−16] capacitive,[17−19] and piezoelectric effects.[20−23] Among these types of pressure sensors, a capacitive pressure sensor takes advantage of its simplicity, low power consumption, and reliable operation.[24−26] However, as the solid elastomer-based capacitance pressure sensor showed poor sensitivity under low pressures, previous research suggested a variety of methods for enhancing the sensitivity of capacitive pressure sensor. These methods are divided into two strategies: (1) microstructuring of elastomers and (2) incorporating high-*k* fillers or conductive fillers to elastomers. First, the microstructuring of elastomers, which leads to enhancing the sensitivity due to a stiffness reduction, were fabricated using three-dimensional microporous structures,[27,28] micropyramid structures,[29,30] microdome structures,[31,32] and micropillar arrays.[33,34] Second, the incorporation of various fillers, including Ag nanowires,[35] Ag nanoparticles,[36] carbon black,[37] $CaCu_3Ti_4O_{12}$,[38] and $BaTiO_3$,[39]

Received: November 5, 2019
Accepted: December 11, 2019
Published: December 11, 2019

Downloaded via KOREA ADVANCED INST SCI AND TECHLGY on November 21, 2022 at 13:35:11 (UTC).
See https://pubs.acs.org/sharingguidelines for options on how to legitimately share published articles.

© 2019 American Chemical Society

DOI: 10.1021/acsami.9b20097
ACS Appl. Mater. Interfaces 2020, 12, 1698−1706

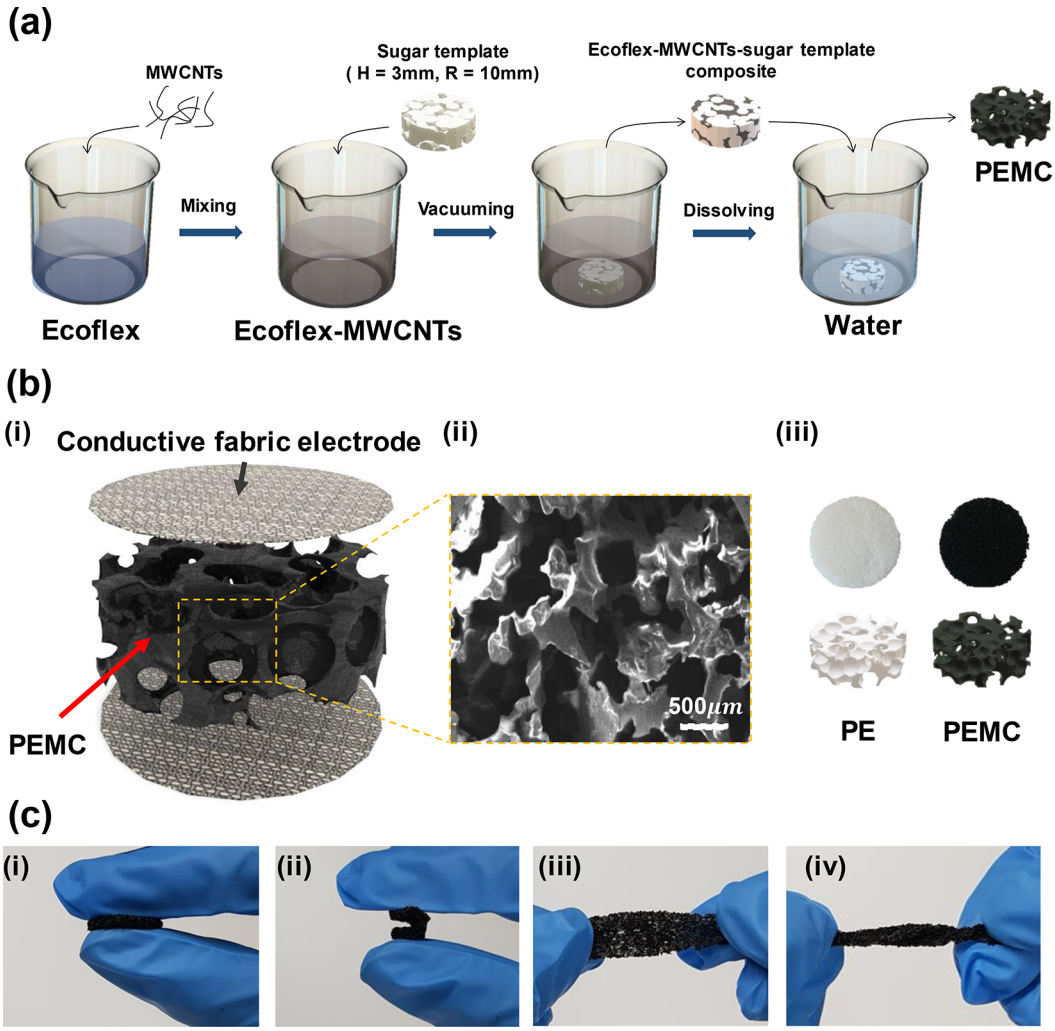


Figure 1. (a) Schematic illustration of the PEMC fabrication process. (b-i) Schematic diagram of the PEMC-based pressure sensor using conductive fabric electrodes. (b-ii) SEM image of the PEMC structure. (b-iii) Photographic images (top view) and 3D modeling images of PE (white) and the PEMC (dark). (c) PEMC structures capable of (i) compression, (ii) bending, (iii) stretching, and (iv) stretch–twist coupling.

into the solid elastomers has been proposed. It is known that the dielectric constant of the composite can be significantly increased by adding a small number of conductive fillers near the percolation threshold as compared to the case of adding high-k fillers. Furthermore, if the conductive filler has a large aspect ratio such as silver nanowires, ε_r can be significantly increased under the compression.[35,36,40,41] The basic principle is based on percolation threshold theory, as reported in the 1970s and 1980s.[42,43] The composite of the solid elastomer and conductive fillers leads to increasing the dielectric constant against applied pressures.

Recently, some researchers introduced the combination of microstructured elastomers and conductive fillers to significantly increase the sensing performance. Liu et al.[36] proposed a method for generating the composite of porous PDMS and Ag NPs. Although the Ag NPs led to increased sensitivity due to the percolation effect of the conductive nanoparticles, this pressure sensor fabricated by using a blowing agent might not reproducibly make the same porosity for different concentrations of Ag nanoparticles due to the variation in viscosity of the PDMS–AgNPs composite. Furthermore, for both methods, as the air trapped inside the composite cannot escape during compression, the composite-based pressure sensor had low sensitivity due to the stiffness of the composite.[44] Following this rationale, it is believed that porous Ecoflex (PE) based on the sugar template,[27] containing conductive fillers such as multiwalled carbon nanotubes (MWCNTs), can yield a high synergetic effect; a sensor constructed on this idea would be of simple fabrication, low cost as compared to other microstructures and fillers, and high suitability for wearable applications. By use of a sugar template, high porosity (~80%) can be attained and air can easily come in and out during compression and release; this can increase the sensitivity and reduce the viscosity of the composite. MWCNTs were used as conductive fillers due to their high strength, oxidation stability, and high aspect ratio, which enable achieving stable responses and reaching the percolation threshold with a small amount of added MWCNTs.

Herein, we introduce simple, cost-effective, and highly sensitive capacitive pressure sensor based on porous the Ecoflex–MWCNTs composite (PEMC), which leads to enhancing the sensitivity due to a synergetic effect of the porous elastomer and percolation of carbon nanotube fillers. The PEMC structure shows excellent mechanical deformability and compliance for an effective integration with practical wearable devices. Furthermore, the PEMC-based pressure

DOI: 10.1021/acsami.9b20097
ACS Appl. Mater. Interfaces 2020, 12, 1698–1706

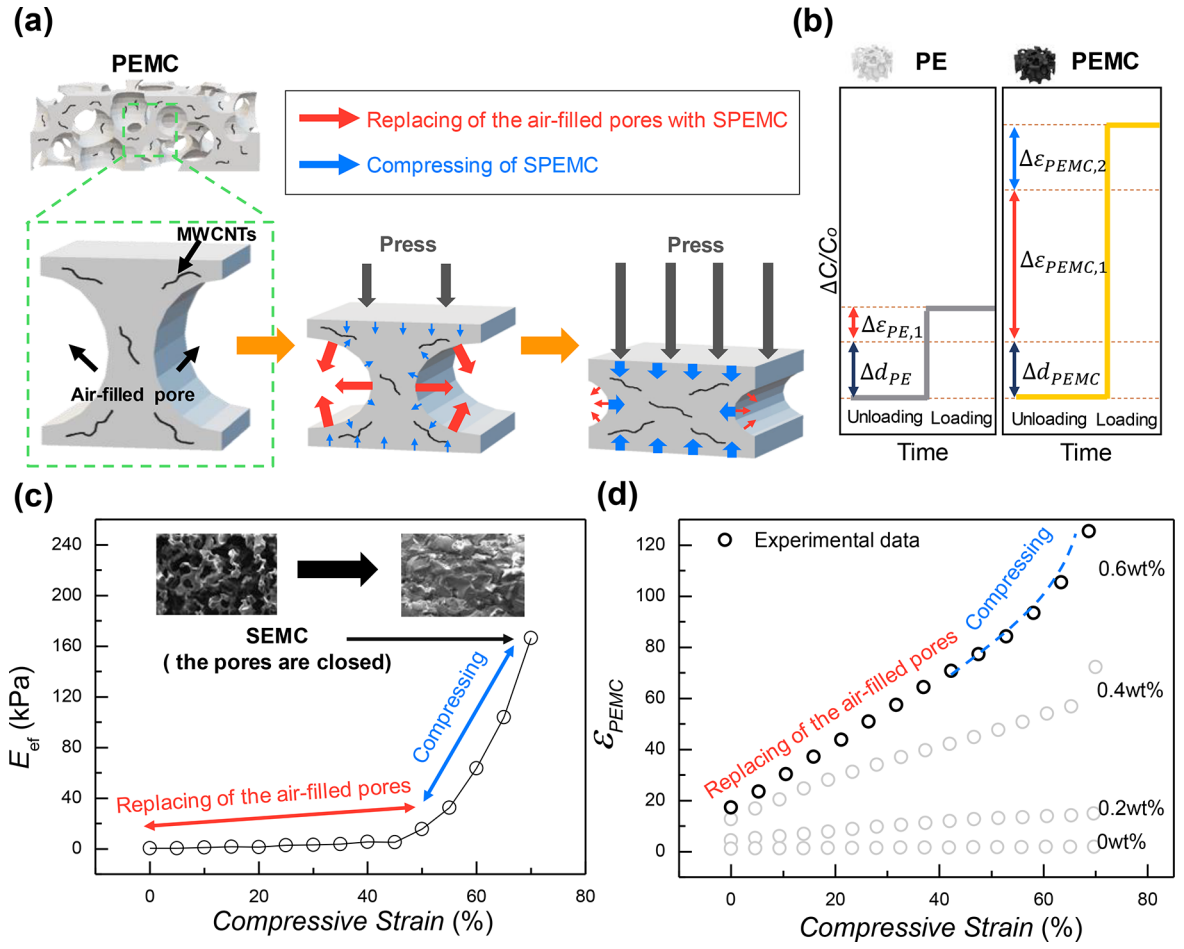


Figure 2. (a) Schematic illustration of structural change of the PEMC under compressive loading. (b) Schematic illustration of $\Delta C/C_0$ of the PE and the PEMC under compressive loading. $\Delta C/C_0$ of the PEMC is much higher than that of the PE due to the change of dielectric constant by the replacement of the air-filled pores ($\Delta\varepsilon_{PEMC,1}$) and the compression the SPEMC ($\Delta\varepsilon_{PEMC,2}$). (c) Relationship between the elastic modulus of the PEMC and compressive strain. The inset shows optical images of the PEMC structure under compressive loading/unloading. (d) Experimental relationship between ε_{PEMC} of the PEMC and compressive strain.

sensor shows not only long-term stability, negligible hysteresis, and rapid response under dynamic loading but also exhibits a highly insensitive property to change in temperature and humidity. Finally, we demonstrated two practical applications integrated with the PEMC-based pressure sensor: a prosthetic robot finger integrated with a PEMC-based pressure sensor and actuator and a healthcare wristband capable of continuously detecting blood pressure and heart rate.

RESULTS AND DISCUSSION

Figure 1a shows a schematic illustration of the PEMC fabrication process, which consists of four steps: mixture of the Ecoflex and MWCNTs, infiltration of the mixture into a sugar template, dissolution of sugars in the water, and generation of the PEMC. The PEMC structures include randomly distributed pores throughout the entire volume, as shown in Figure 1b(i). In Figure 1b(ii), the scanning electron microscope (SEM) image shows the morphology of the PEMC, in which the pore size was observed to be 288 ± 85 μm and the porosity was calculated as a value of 80.56 ± 0.84% (Figure S1 and Table S1). Figure 1b(iii) shows the photographic images of the porous Ecoflex (white) and the PEMC (dark), respectively. The PEMC structure provides an excellent flexibility and compressibility, which facilitates pressing, bending, stretching, and stretch–twist coupling, respectively, as depicted in Figure 1c.

In general, the capacitance between two large parallel electrodes is defined as $C = \varepsilon_0\varepsilon_r(A/d)$, where ε_0 is permittivity of space and ε_r is dielectric constant, d is the distance between electrodes, and A is the overlapping area between electrodes. The normalized capacitance change ($\Delta C/C_0$) can be expressed as $\frac{\Delta C}{C_0} = \frac{\varepsilon'}{\varepsilon}\frac{d}{d'} - 1$, where ε, d and ε', d' are dielectric constant and distance between electrodes before and after the compression, respectively. For the PE and PEMC structures, the distance change is almost the same due to negligible difference of stiffness, as shown in Figure S2. Thus, $\Delta C/C_0$ is mainly governed by a dominant term, $\varepsilon'_{PEMC}/\varepsilon_{PEMC}$. Figure 2a shows a schematic illustration of the structural deformation of the PEMC during the compressive loading. The structural deformation leads to increasing $\varepsilon'_{PEMC}/\varepsilon_{PEMC}$, which depends on the replacement of the low dielectric constant (air, $\varepsilon_{air} = 1$) with the high dielectric constant of a solid part of the PEMC (SPEMC) and the compression of the SPEMC. Figure 2b shows a schematic illustration of $\Delta C/C_0$ of the PE and PEMC under the compressive loading, respectively. $\Delta C/C_0$ of the PEMC is much higher than that of the PE due to the change of the dielectric constant generated from both the replacement of the air-filled pores ($\Delta\varepsilon_{p,1}$) and the compression of the SPEMC

DOI: 10.1021/acsami.9b20097
ACS Appl. Mater. Interfaces 2020, 12, 1698−1706

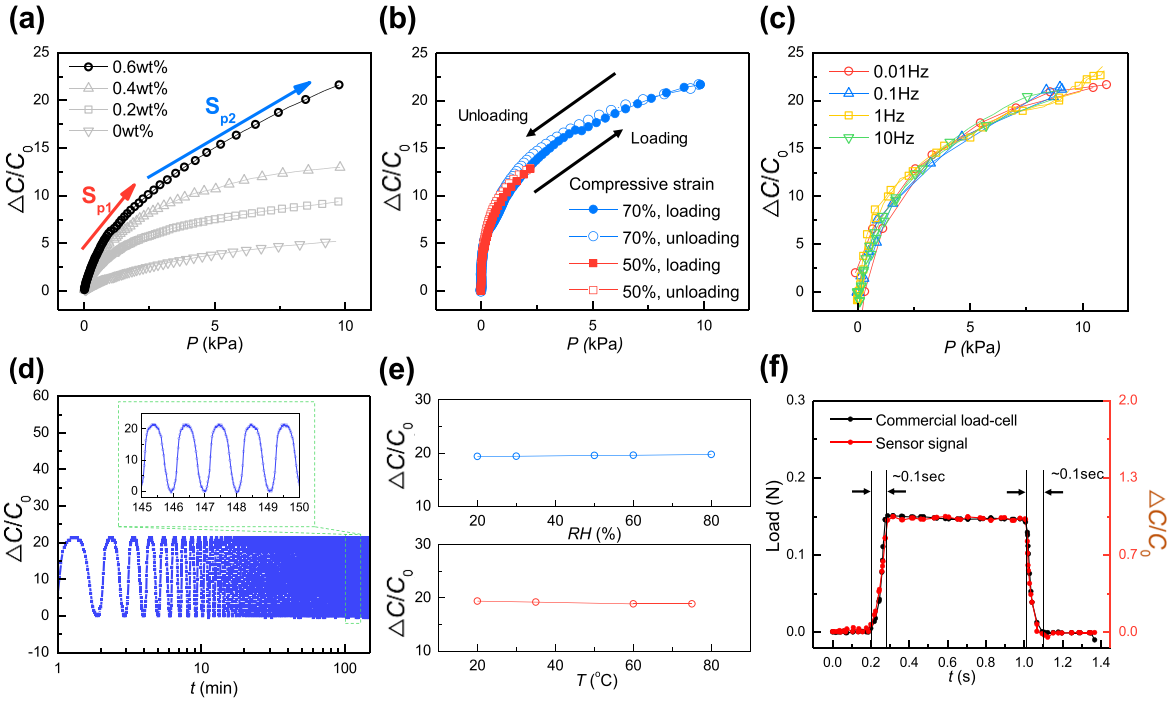


Figure 3. (a) Performance of the PEMC-based pressure sensors with different concentrations of MWCNTs. (b) Hysteresis characteristics of the PEMC-based pressure sensor for the compressive strain up to 70%. (c) Dynamic responses of the PEMC-based pressure sensor for the pressure of 10 kPa and the frequency up to 10 Hz. (d) Long-term electromechanical stability of the PEMC-based pressure sensor over 10000 cycles of a repeated compression/release test with a compressive strain of 70%. (e) $\Delta C/C_0$ of the PEMC-based pressure sensor under different temperature and humidity conditions. (f) $\Delta C/C_0$ of the PEMC-based pressure sensor vs time with a commercial load cell.

($\Delta\varepsilon_{p,2}$). Figure 2c shows the effective elastic modulus (E_{ef}) of the PEMC at different values of the compressive strain. E_{ef} increased linearly until the compressive strain of 50% due to the replacement of air with SPEMC, while it sharply increased at the compressive strain ranged from 50 to 70% due to both the replacement of air with SPEMC and its compression. Here, E_{ef} of the PEMC structure at the compressive strain of 70% showed the same value as that of the SEMC. The inset shows the optical images of the PEMC structures under compressive unloading and loading, respectively. To understand the sensing mechanism of the PEMC-based pressure sensor, we expressed a theoretical relationship between the dielectric constant and the strain of the PEMC using Maxwell's equation[45] as explained in eqs S1 and S2 and Figure S3 in the Supporting Information. In Figure 2d, as ε_{solid} is constant up to the compressive strain of 50%, ε_{PEMC} increased linearly. On the other hand, ε_{PEMC} increased exponentially with ε_{solid} at the compressive strain of 50−70% according to the power law of percolation theory.[25,35,46,47]

Figure 3a shows the pressure-sensing performance of the PEMC-based pressure sensor. $\Delta C/C_0$ under applied pressures was compared between different weight percents (0−0.6 wt %) of MWCNTs. The sensitivity (S) of the PEMC-based pressure sensor is defined as the slope of the curve ($S = \delta(\Delta C/C_0)/\delta P$), which consists of two different steps (0−2 and 2−10 kPa). In both steps, the PEMC-based pressure sensor with 0.6 wt % of MWCNTs showed an excellent pressure-sensing performance with high sensitivity (S_{p1} = 6.42 kPa^{-1}), which is nearly 4 times higher than that of the pressure sensor obtained by the PE-based pressure sensor. In the first step, this high sensitivity can be explained by the fact that the initial high number of pores in PEMC is replaced rapidly by the high dielectric constant elastomer (SPEMC) upon compression. In the second step of the pressure response, the sensitivity is observed to be higher for the higher values of MWCNTs. This sensitivity can be explained by the fact that the distribution of MWCNTs is denser as the PEMC is compressed. For the static and dynamic response tests, the PEMC-based pressure sensor shows negligible hysteresis at the compressive strain up to 70% and the frequency up to 10 Hz, respectively, as shown in Figures 3b and 3c. This can be explained by the fact that pores within the whole volume of the PEMC can reduce the volume fraction of the elastomer. As the existence of pores led to reducing the viscoelastic property of the SEMC, a reversible sensor response could be achieved without noticeable hysteresis.[48,49] We also confirmed these viscoelastic properties of SEMC and PEMC using the standard solid model; a spring and the Kelvin−Voigt model are connected in series (Figures S4 and S5). In Figure 3d, the long-term stability and electromechanical durability of the PEMC were evaluated under 10000 cycles of repeated compression/release at ∼10 kPa (compressive strain of 70%). No drift of the sensor response and no structural change of the PEMC were found during the cycles. From the results, it was confirmed that the sensor is appropriate for long-term, repeated health monitoring applications such as real-time wrist pulse measurement. In Figure 3e, the PEMC-based pressure sensor was evaluated at different values of temperature and humidity. As temperature (T) increased from 20 to 75 °C, $\Delta C/C_0$ of the pressure sensor was not significantly fluctuated. This means that the sensor can be used for practical wearable devices because most of the electrical devices for these purposes should not exceed 65 °C in general. Also, when the RH changed from 15 to 90%, a variation in $\Delta C/C_0$ was not observed. The response time and recovery time of the PEMC-based pressure sensor were examined as shown in Figure 3f. Because the actuator cannot generate an ideal step displace-

DOI: 10.1021/acsami.9b20097
ACS Appl. Mater. Interfaces 2020, 12, 1698−1706

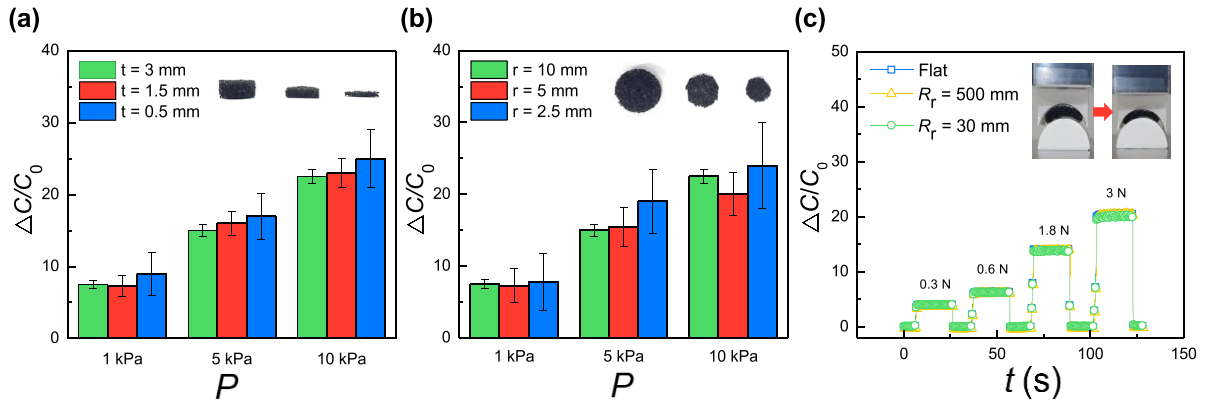


Figure 4. (a, b) Pressure sensing performance of the PEMC-based pressure sensors with different thicknesses (3, 1.5, and 0.5 mm) and radii (10, 5, and 2.5 mm). (c) Pressure sensing performances of the PEMC-based pressure sensor under different curvature radii of ∞, 50 mm, and 30 mm.

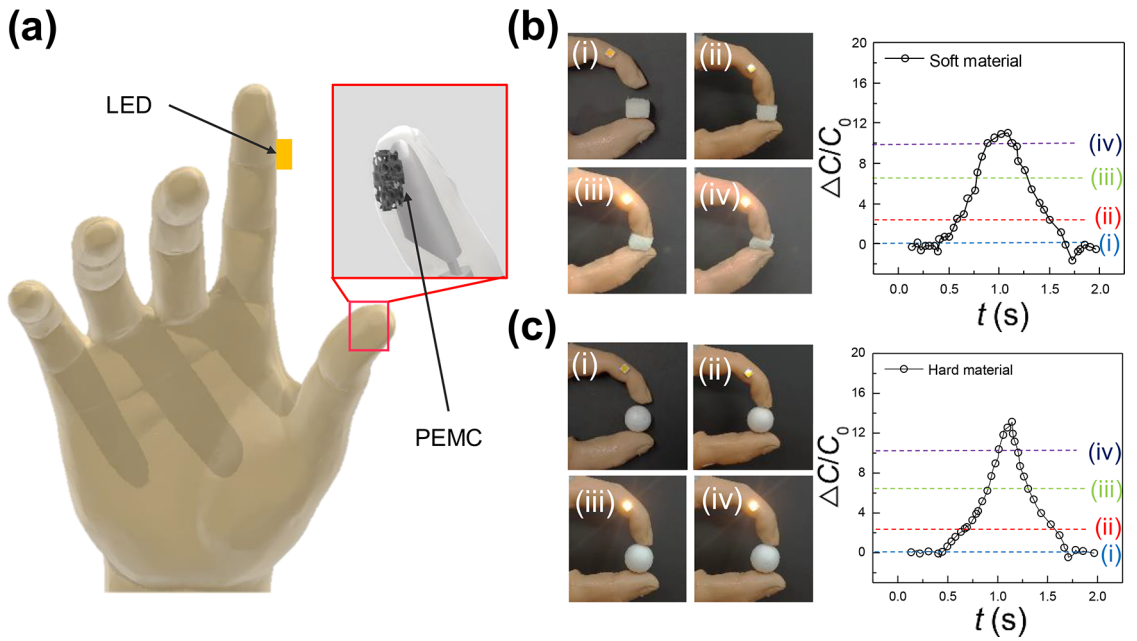


Figure 5. (a) 3D model of the constructed prosthetic arm, with an integrated robot finger for grasping movements; an LED is attached to the index finger to gauge the pressure sensed by the PEMC-based pressure sensor embedded into the thumb. Demonstration of the grasping abilities of the robot finger for (b) a soft material (PE) and (c) a hard material (plastic ball).

ment, we are not able to accurately calculate the response and recovery times of the sensor. Instead, we compared the transient response of our sensor to that of the commercial load cell. From this result, we could conclude that the PEMC-based pressure sensor operates as fast as a commercial load cell with response and recovery times shorter than at least 0.1 s.

For wearable devices, the dimensions of the soft sensors are important factors for better wearability and less interference with diverse human motions. As shown in Figures 4a and 4b, the pressure-sensing performances of the PEMC-based pressure sensor were examined for different values of thickness and radius of the PEMC structure. The PEMC-based pressure sensor showed a similar response against the applied pressure regardless of sensor dimensions. Also, the PEMC-based pressure sensor should be evaluated under bending stimuli for use in wearable applications. In Figure 4c, $\Delta C/C_0$ of the PEMC-based pressure sensor were compared at $r_{bending}$ of ∞, 30 mm, and 500 mm, respectively. The sensing characteristics of the PEMC-based pressure sensor on a flat surface was used as a reference. The applied stimuli were denoted as normal forces, as the effective contact area was not well-defined. The PEMC-based pressure sensor over $r_{bending}$ of 30 mm showed bending-insensitive properties under different forces (0.3, 0.6, 1.8, and 3 N). Also, the PEMC-based pressure sensor did not show any mechanical or electrical failure during the bending stimuli due to intrinsic active materials.[50]

From the excellent sensor properties, we applied the PEMC-based pressure sensor for the prosthetic robot finger and the healthcare wristband. For the prosthetic robot finger, Ecoflex was used for the integration of the PEMC-based sensor within a prosthetic robot finger given that it is one of the most skinlike elastomers. The motion of the prosthetic finger was controlled by a fabric glove with a piezoresistive strain sensor attached to it. Figure 5a shows a 3D model of the constructed prosthetic arm, with the integrated robot finger for grasping movements; a light-emitting diode (LED) was attached to the index finger to gauge the pressure sensed by the PEMC-based pressure sensor embedded into the thumb. As shown in Figure

DOI: 10.1021/acsami.9b20097
ACS Appl. Mater. Interfaces 2020, 12, 1698−1706

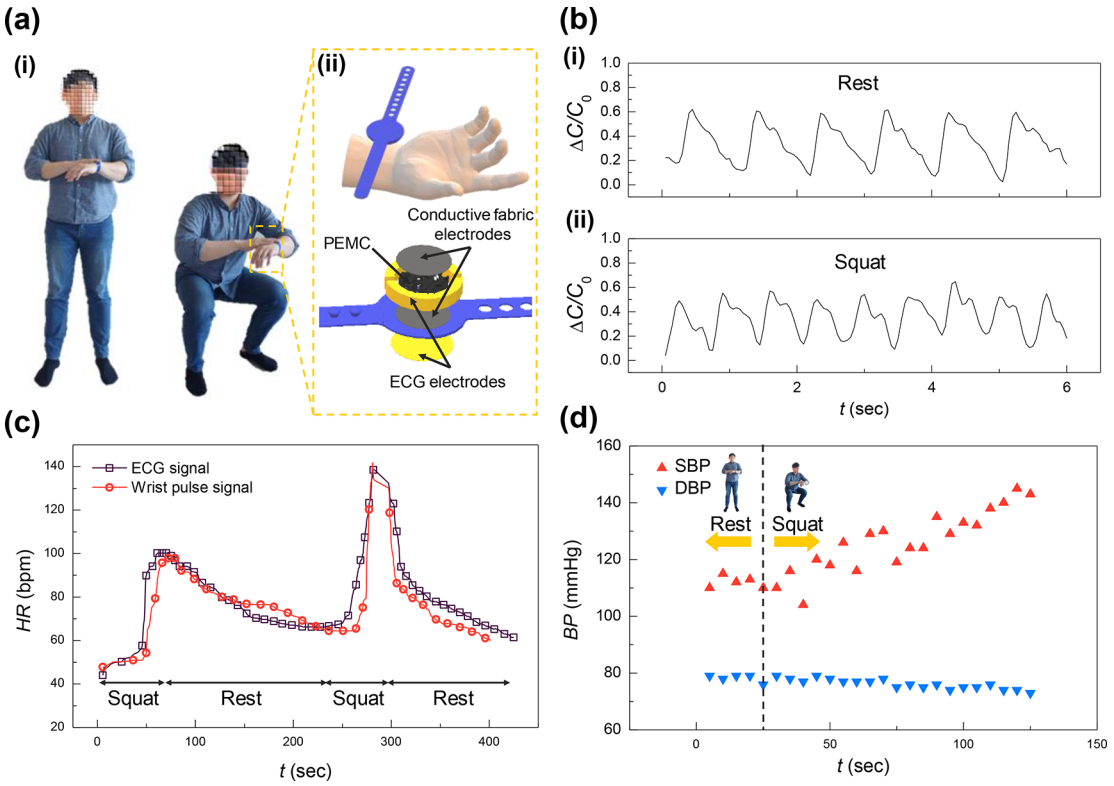


Figure 6. (a-i) Photographic images of a person wearing the healthcare wristband for epidermal pulse rate monitoring in resting position (left) and squatting position (right). (a-ii) Schematics depicting the components of the wristband. (b) Comparison of wrist pulse signals (i) before and (ii) after the squat. (c) HR during exercise from the PEMC-based pressure sensor and the ECG sensor. The HR from the PEMC-based pressure sensor showed great match to the reference heart rate from the ECG sensor. (d) Time delay between the signals from the PEMC-based pressure sensor and the ECG sensor (i.e., pulse transmit time (PTT)) is used to estimate the blood pressure as shown in Figure S5. By use of the relationship between PTT and BP,[51,52] the BP (systolic blood pressure (SBP) and diastolic blood pressure (DBP)) could be estimated. During the exercise, an increase in the SBP and a slight decrease in the DBP are observed.

5b,c, the LED brightened up as increasing pressure was applied onto the thumb; here, we demonstrated the grabbing of PE as a soft material (Figure 5b) and a plastic ball (Figure 5c) as a hard material. As shown in Movie S1 and Movie S2, we have demonstrated the feasibility of the PEMC-based pressure sensor in a smart prosthetic hand capable of stable, continuous, and accurate detection of low-pressure stimuli.

The PEMC-based pressure sensor could also be applied to a human healthcare monitoring system. The heart rate (HR) and blood pressure (BP) of an individual were monitored during resting and squatting positions as shown in Figure 6a through a healthcare wristband, which integrated an electrocardiogram (ECG) sensor and the PEMC-based pressure sensor. The healthcare wristband is composed of two ECG electrodes, two conductive fabric electrodes (Knit Jersey Conductive Fabric, Adafruit, USA), the PEMC, and a control board. The fast response and high sensitivity of the PEMC-based pressure sensor enable the high-resolution measurement of pulse waves in Figure 6b for the resting and squatting positions. From this figure, HR could be estimated by measuring the time difference between two peak points of the wrist pulse signals. As expected, the HR obtained from the interval time of the wrist signal is faster during the exercise. To validate the HR from the PEMC-based pressure sensor on wristband, this value was compared to the HR from the ECG signal (Movie S3), also integrated on the wristband, during exercise as shown in Figure 6c. The data taken from both the PEMC-based pressure sensor and ECG were in good agreement. In Figure S6, the time delay between the blood pulse signal from the PEMC-based pressure sensor and the electrical activity of the heart from ECG is defined as pulse transmit time (PTT). By use of the relationship between PTT and BP, the BP could be estimated as previously reported for blood pressure estimation.[51] In Figure 6d, the systolic blood pressure (SBP) and the diastolic blood pressure (DBP), which are important factors in human healthcare application, were calculated by using the PPT−BP relation in ref 52. The validity of the blood pressure change from the measured data can be confirmed by the medical fact in the literature.[53]

CONCLUSION

In summary, we demonstrated a simple, cost-effective, wearable capacitive pressure sensor based on the PEMC structure, which provided excellent mechanical properties for an effective integration with practical wearable devices. The PEMC-based pressure sensor showed a high sensitivity with negligible hysteresis in the low-pressure regime due to a synergy effect of the porous elastomer and the existence of conductive fillers. Also, it exhibited the long-term stability and fast response under dynamic loading as well as the high stability against temperature and humidity changes. Finally, we demonstrated that the PEMC-based pressure sensor could be applied to the prosthetic robot finger and the healthcare wristband. We believe that this strategy can provide a useful approach to achieve accurate detection and real-time monitoring in the low-pressure regime for use in a variety of

DOI: 10.1021/acsami.9b20097
ACS Appl. Mater. Interfaces 2020, 12, 1698−1706

wearable applications such as the development of tactile sensors, human motion detection, human−machine interaction, electronic skins for soft robotics, and wearable pressure-sensing devices for health diagnosis systems.

EXPERIMENTAL SECTION

Fabrication of Cylindrically Shaped Sugar Template. A cylindrically shaped master mold for generation of a sugar template was fabricated by using a 3D printer (Ulitmaker3, USA). Sugar powders were poured into the cylindrically shaped master mold. After pressing on sugar powder, the sugar template was dried in a convection oven at 100 °C for 12 h. Finally, the cylindrically shaped sugar template was detached from the master mold.

Preparation of PEMC. There are two components for the Ecoflex00-30 prepolymer solution (Smooth-On, USA): a base and a curing agent. They were mixed individually with the same concentration of MWNTs (Hanwha, KOREA) due to the short curing time of Ecoflex. A planetary mixer was used to make the MWNTs well dispersed in each of the prepolymer solutions. The "base−MWNTs mixture" and the "curing agent−MWNTs mixture" were mixed together by using a planetary mixer with a weight ratio of 1:1. A mixture of Ecoflex00-30 prepolymers and MWCNTs was infiltrated into the cylindrically shaped sugar templates in a vacuum chamber and then cured at room temperature for 5 h. The composite of sugar template−Ecoflex−MWCNTs was immersed in water to dissolve the sugar portion for the fabrication of PEMC.

Characterization of Sensor Response. A high-precision universal testing machine (AGS-X, Shimadzu, Japan) was used to evaluate the sensing performances. A disk-type compression fixture with a diameter of 40 mm was utilized for uniform deformation of the sensor. A position-controlled compression test was conducted at a compressive speed of 0.05 mm s^{-1}. During the compression, the capacitance of the sensor was measured by using LCR meter (E4980A, Agilent, USA) at a frequency of 100 kHz. To measure the response and recovery time, a microactuator (MA-35, Physik Instrumente, Germany) and a force transducer (SM-500N, Interface, USA) were used under a position-controlled compression with a compressive speed of 5 mm s^{-1}. Temperature and humidity were monitored by using an IR camera (E30, FLIR, USA) and a humidity sensor (SHT31 SMART, Sensiron, USA), respectively (Figure S7). Also, a shaker (K2002E01, THE MODAL SHOP, USA) was employed to evaluate the dynamic responses of the pressure sensor at different strain rates of the sensors. The shaker was vibrated with a function generator that provided specific strain rates.

Fabrication of Prosthetic Robot Finger. A prosthetic robot finger was fabricated by first building its skeleton and then covering it with a thin skinlike elastomer. For the first part, a human hand was scanned by a 3D scanner (XYZ Printing, Taiwan) for modeling the skeleton of the robot fingers. After that, the skeleton of the robot fingers was printed by a 3D printer using thermoplastic polyurethane. The robot finger was then connected to a servo motor (DM-S0300D, China) with threads for its actuation (Figure S8). For the second part, a thin skinlike elastomer was fabricated by the following three sequential steps. First, Alja Safe powder (Smooth-On, USA) was mixed with water to form a rubbery elastomer, which was subsequently poured into a container. Second, human fingers were dipped into the container for 5 min until it was cured to form a mold for the skinlike elastomer. Finally, Ecoflex00-35 prepolymers (Smooth-On, USA) were poured into the mold back and forth to form the thin skinlike film conformably around the mold (Figure S9).

Fabrication of System for Wearable Device. For both the prosthetic robot finger and the healthcare wristband, a capacitance to digital converter (CDC, FDC1004, Texas Instruments, USA) was used instead of an LCR meter, as this allows for more compact and lightweight applications. This CDC can also shield the sensor from environmental interferences by using an out-of-phase electrical model (Figure S10). Additionally, for the healthcare wristband, an ECG sensor (PSL-iECG2, PhysioLab, KOREA) was employed, which provides three pins to attach on the human skin for obtaining the ECG signal. Furthermore, both the CDC and ECG sensors were controlled with an Arduino Uno using an I2C standard interface with a rate of 100 samples per second (SPS).

ASSOCIATED CONTENT

Supporting Information

The Supporting Information is available free of charge at https://pubs.acs.org/doi/10.1021/acsami.9b20097.

Porosity and pore size of the PEMC structure; compressive strain−pressure curves of the SEMC and the PEMC with different concentrations of MWCNTs; viscoelastic properties of the PEMC structure; pulse transit time between the blood pulse signal from the PEMC-based wristband and ECG; experimental setup for testing the PEMC-based pressure sensor at various temperatures; fabrication of the prosthetic robot fingers; shielding method for the PEMC-based capacitive pressure sensor (PDF)

Movie S1: pressure signal monitoring of the PEMC-based pressure sensor embedded into the thumb of the prosthetic robot finger during actuation (MP4)

Movie S2: demonstration a person controlling the prosthetic robot finger while monitoring the pressure sensed by the robot finger through an LED (MP4)

Movie S3: pulse wave signal from the PEMC-based pressure sensor on the wrist and the ECG signal (MP4)

AUTHOR INFORMATION

Corresponding Authors

*E-mail: inkyu@kaist.ac.kr.

*E-mail: oyongsuk@kaist.ac.kr.

ORCID

Inkyu Park: 0000-0001-5761-7739

Notes

The authors declare no competing financial interest.

ACKNOWLEDGMENTS

This work was supported by the National Research Foundation of Korea (NRF) grant funded by the Korea government (MSIT) (No. 2018R1A2B2004910) and the National Research Foundation of Korea (NRF) Grant funded by the Korean Government (MSIP) (No. 2015R1A5A1037668). This research was also supported by the KUSTAR-KAIST Institute, KAIST, Korea.

REFERENCES

(1) Boutry, C. M.; Nguyen, A.; Lawal, Q. O.; Chortos, A.; Rondeau-Gagné, S.; Bao, Z. A Sensitive and Biodegradable Pressure Sensor Array for Cardiovascular Monitoring. *Adv. Mater.* **2015**, *27*, 6954.

(2) Song, Y.; Huang, W.; Mu, C.; Chen, X.; Zhang, Q.; Ran, A.; Peng, Z.; Sun, R.; Xie, W. Carbon Nanotube-Modified Fabric for Wearable Smart Electronic-Skin with Exclusive Normal-Tangential Force Sensing Ability. *Adv. Mater. Technol.* **2019**, *4*, 1800680.

(3) Takeuchi, K.; Kim, B. Functionalized Microneedles for Continuous Glucose Monitoring. *Nano Convergence.* **2018**, DOI: 10.1186/s40580-018-0161-2.

(4) Boutry, C. M.; Nguyen, A.; Lawal, Q. O.; Chortos, A.; Rondeau-Gagné, S.; Bao, Z. A Sensitive and Biodegradable Pressure Sensor Array for Cardiovascular Monitoring. *Adv. Mater.* **2015**, *27* (43), 6954−6961.

(5) Roh, E.; Hwang, B. U.; Kim, D.; Kim, B. Y.; Lee, N. E. Stretchable, Transparent, Ultrasensitive, and Patchable Strain Sensor for Human-Machine Interfaces Comprising a Nanohybrid of Carbon

DOI: 10.1021/acsami.9b20097
ACS Appl. Mater. Interfaces 2020, 12, 1698−1706

Nanotubes and Conductive Elastomers. *ACS Nano* **2015**, *9* (6), 6252−6261.
(6) Zhong, J.; Ma, Y.; Song, Y.; Zhong, Q.; Chu, Y.; Karakurt, I.; Bogy, D. B.; Lin, L. A Flexible Piezoelectret Actuator/Sensor Patch for Mechanical Human-Machine Interfaces. *ACS Nano* **2019**, *13*, 7107.
(7) Lim, S.; Son, D.; Kim, J.; Lee, Y. B.; Song, J. K.; Choi, S.; Lee, D. J.; Kim, J. H.; Lee, M.; Hyeon, T.; Kim, D. H. Transparent and Stretchable Interactive Human Machine Interface Based on Patterned Graphene Heterostructures. *Adv. Funct. Mater.* **2015**, *25* (3), 375−383.
(8) Lee, J.; Kwon, H.; Seo, J.; Shin, S.; Koo, J. H.; Pang, C.; Son, S.; Kim, J. H.; Jang, Y. H.; Kim, D. E.; Lee, T. Conductive Fiber-Based Ultrasensitive Textile Pressure Sensor for Wearable Electronics. *Adv. Mater.* **2015**, *27* (15), 2433−2439.
(9) Dong, K.; Wang, Y. C.; Deng, J.; Dai, Y.; Zhang, S. L.; Zou, H.; Gu, B.; Sun, B.; Wang, Z. L. A Highly Stretchable and Washable All-Yarn-Based Self-Charging Knitting Power Textile Composed of Fiber Triboelectric Nanogenerators and Supercapacitors. *ACS Nano* **2017**, *11* (9), 9490−9499.
(10) Di, J.; Zhang, X.; Yong, Z.; Zhang, Y.; Li, D.; Li, R.; Li, Q. Carbon-Nanotube Fibers for Wearable Devices and Smart Textiles. *Adv. Mater.* **2016**, *28* (47), 10529−10538.
(11) Pang, Y.; Zhang, K.; Yang, Z.; Jiang, S.; Ju, Z.; Li, Y.; Wang, X.; Wang, D.; Jian, M.; Zhang, Y.; Liang, R.; Tian, H.; Yang, Y.; Ren, T.-L. Epidermis Microstructure Inspired Graphene Pressure Sensor with Random Distributed Spinosum for High Sensitivity and Large Linearity. *ACS Nano* **2018**, *12*, 2346.
(12) Park, K.; Kim, S.; Lee, H.; Park, I.; Kim, J. Low-Hysteresis and Low-Interference Soft Tactile Sensor Using a Conductive Coated Porous Elastomer and a Structure for Interference Reduction. *Sens. Actuators, A* **2019**, *295*, 541.
(13) Lee, H.; Kwon, D.; Cho, H.; Park, I.; Kim, J. Soft Nanocomposite Based Multi-Point, Multi-Directional Strain Mapping Sensor Using Anisotropic Electrical Impedance Tomography. *Sci. Rep.* **2017**, DOI: 10.1038/srep39837.
(14) Song, Y.; Huang, W.; Mu, C.; Chen, X.; Zhang, Q.; Ran, A.; Peng, Z.; Sun, R.; Xie, W. Carbon Nanotube-Modified Fabric for Wearable Smart Electronic-Skin with Exclusive Normal-Tangential Force Sensing Ability. *Adv. Mater. Technol.* **2019**, *4*, 1800680.
(15) Mu, C.; Song, Y.; Huang, W.; Ran, Ao; Sun, R.; Xie, W.; Zhang, H. Flexible Normal-Tangential Force Sensor with Opposite Resistance Responding for Highly Sensitive Artificial Skin. *Adv. Funct. Mater.* **2018**, *28*, 1707503.
(16) Sencadas, V.; Tawk, C.; Alici, G. Highly Sensitive Soft Foam Sensors to Empower Robotic Systems. *Adv. Mater. Technol.* **2019**, *4*, 1900423.
(17) Cho, S. H.; Lee, S. W.; Yu, S.; Kim, H.; Chang, S.; Kang, D.; Hwang, I.; Kang, H. S.; Jeong, B.; Kim, E. H.; Cho, S. M.; Kim, K. L.; Lee, H.; Shim, W.; Park, C. Micropatterned Pyramidal Ionic Gels for Sensing Broad-Range Pressures with High Sensitivity. *ACS Appl. Mater. Interfaces* **2017**, *9*, 10128.
(18) Viry, L.; Levi, A.; Totaro, M.; Mondini, A.; Mattoli, V.; Mazzolai, B.; Beccai, L. Flexible Three-Axial Force Sensor for Soft and Highly Sensitive Artificial Touch. *Adv. Mater.* **2014**, *26*, 2659.
(19) Kim, J. O.; Kwon, S. Y.; Kim, Y.; Choi, H. B.; Yang, J. C.; Oh, J.; Lee, H. S.; Sim, J. Y.; Ryu, S.; Park, S. Highly Ordered 3D Microstructure-Based Electronic Skin Capable of Differentiating Pressure, Temperature, and Proximity. *ACS Appl. Mater. Interfaces* **2019**, *11*, 1503.
(20) Kim, K.; Park, J.; Suh, J.; Kim, M.; Jeong, Y.; Park, I. 3D Printing of Multiaxial Force Sensors Using Carbon Nanotube (CNT)/Thermoplastic Polyurethane (TPU) Filaments. *Sens. Actuators, A* **2017**, *263*, 493.
(21) Zhu, J.; Zhu, Y.; Song, W.; Wang, H.; Gao, M.; Cho, M.; Park, I. Zinc Oxide-Enhanced Piezoelectret Polypropylene Microfiber for Mechanical Energy Harvesting. *ACS Appl. Mater. Interfaces* **2018**, *10*, 19940.
(22) Pan, C.; Dong, L.; Zhu, G.; Niu, S.; Yu, R.; Yang, Q.; Liu, Y.; Wang, Z. L. High-Resolution Electroluminescent Imaging of Pressure Distribution Using a Piezoelectric Nanowire LED Array. *Nat. Photonics* **2013**, *7*, 752.
(23) Dagdeviren, C.; Su, Y.; Joe, P.; Yona, R.; Liu, Y.; Kim, Y.-S.; Huang, Y.; Damadoran, A. R.; Xia, J.; Martin, L. W.; Huang, Y.; Rogers, J. A. Conformable Amplified Lead Zirconate Titanate Sensors with Enhanced Piezoelectric Response for Cutaneous Pressure Monitoring. *Nat. Commun.* **2014**, DOI: 10.1038/ncomms5496.
(24) Wang, X.; Li, T.; Adams, J.; Yang, J. Transparent, Stretchable, Carbon-Nanotube-Inlaid Conductors Enabled by Standard Replication Technology for Capacitive Pressure, Strain and Touch. *J. Mater. Chem. A* **2013**, *1*, 3580.
(25) Kim, S. Y.; Park, S.; Park, H. W.; Park, D. H.; Jeong, Y.; Kim, D. H. Highly Sensitive and Multimodal All-Carbon Skin Sensors Capable of Simultaneously Detecting Tactile and Biological Stimuli. *Adv. Mater.* **2015**, *27*, 4178.
(26) Yao, S.; Zhu, Y. Wearable Multifunctional Sensors Using Printed Stretchable Conductors Made of Silver Nanowires. *Nanoscale* **2014**, *6*, 2345.
(27) Kwon, D.; Lee, T. I.; Shim, J.; Ryu, S.; Kim, M. S.; Kim, S.; Kim, T. S.; Park, I. Highly Sensitive, Flexible, and Wearable Pressure Sensor Based on a Giant Piezocapacitive Effect of Three-Dimensional Microporous Elastomeric Dielectric Layer. *ACS Appl. Mater. Interfaces* **2016**, *8*, 16922.
(28) Atalay, O.; Atalay, A.; Gafford, J.; Walsh, C. A Highly Sensitive Capacitive-Based Soft Pressure Sensor Based on a Conductive Fabric and a Microporous Dielectric Layer. *Adv. Mater. Technol.* **2018**, *3*, 1700237.
(29) Choong, C.-L.; Shim, M.-B.; Lee, B.-S.; Jeon, S.; Ko, D.-S.; Kang, T.-H.; Bae, J.; Lee, S. H.; Byun, K.-E.; Im, J.; Jeong, Y. J.; Park, C. E.; Park, J.-J.; Chung, U-I. Highly Stretchable Resistive Pressure Sensors Using a Conductive Elastomeric Composite on a Micropyramid Array. *Adv. Mater.* **2014**, *26*, 3451.
(30) Deng, W.; Huang, X.; Chu, W.; Chen, Y.; Mao, L.; Tang, Q.; Yang, W. Microstructure-Based Interfacial Tuning Mechanism of Capacitive Pressure Sensors for Electronic Skin. *J. Sens.* **2016**, *2016*, 1.
(31) Park, J.; Lee, Y.; Hong, J.; Ha, M.; Jung, Y.; Do; Lim, H.; Kim, S. Y.; Ko, H. Giant Tunneling Piezoresistance of Composite Elastomers with Interlocked Microdome Arrays for Ultrasensitive and Multimodal Electronic Skins. *ACS Nano* **2014**, *8*, 4689.
(32) Zhang, Y.; Hu, Y.; Zhu, P.; Han, F.; Zhu, Y.; Sun, R.; Wong, C. P. Flexible and Highly Sensitive Pressure Sensor Based on Microdome-Patterned PDMS Forming with Assistance of Colloid Self-Assembly and Replica Technique for Wearable. *ACS Appl. Mater. Interfaces* **2017**, *9*, 35968.
(33) Park, H.; Jeong, Y. R.; Yun, J.; Hong, S. Y.; Jin, S.; Lee, S. J.; Zi, G.; Ha, J. S. Stretchable Array of Highly Sensitive Pressure Sensors Consisting of Polyaniline Nanofibers and Au-Coated Polydimethylsiloxane Micropillars. *ACS Nano* **2015**, *9*, 9974.
(34) Chen, X.; Li, X.; Shao, J.; An, N.; Tian, H.; Wang, C.; Han, T.; Wang, L.; Lu, B. High-Performance Piezoelectric Nanogenerators with Imprinted P(VDF-TrFE)/BaTiO3 Nanocomposite Micropillars for Self-Powered Flexible Sensors. *Small* **2017**, *13*, 1604245.
(35) Wang, J.; Jiu, J.; Nogi, M.; Sugahara, T.; Nagao, S.; Koga, H.; He, P.; Suganuma, K. A Highly Sensitive and Flexible Pressure Sensor with Electrodes and Elastomeric Interlayer Containing Silver Nanowires. *Nanoscale* **2015**, *7*, 2926.
(36) Liu, S. Y.; Lu, J. G.; Shieh, H. P. D. Influence of Permittivity on the Sensitivity of Porous Elastomer-Based Capacitive Pressure Sensors. *IEEE Sens. J.* **2018**, *18*, 1870.
(37) Guo, X.; Huang, Y.; Cai, X.; Liu, C.; Liu, P. Capacitive Wearable Tactile Sensor Based on Smart Textile Substrate with Carbon Black /Silicone Rubber Composite Dielectric. *Meas. Sci. Technol.* **2016**, *27*, 045105.
(38) Mu, C.; Li, J.; Song, Y.; Huang, W.; Ran, A.; Deng, K.; Huang, J.; Xie, W.; Sun, R.; Zhang, H. Enhanced Piezocapacitive Effect in CaCu 3 Ti 4 O 12 − Polydimethylsiloxane Composited Sponge for

DOI: 10.1021/acsami.9b20097
ACS Appl. Mater. Interfaces 2020, 12, 1698−1706

Ultrasensitive Flexible Capacitive Sensor. *ACS Appl. Nano Mater.* **2018**, *1*, 274.
(39) Cholleti, E. R.; Stringer, J.; Assadian, M.; Battmann, V.; Bowen, C.; Aw, K. Highly Stretchable Capacitive Sensor with Printed Carbon Black Electrodes on Barium Titanate Elastomer Composite. *Sensors* **2019**, *19*, 42.
(40) Shi, R.; Lou, Z.; Chen, S.; Shen, G. Flexible and Transparent Capacitive Pressure Sensor with Patterned Microstructured Composite Rubber Dielectric for Wearable Touch Keyboard Application. *Sci. China Mater.* **2018**, *61*, 1587.
(41) Cui, J.; Zhang, B.; Duan, J.; Guo, H.; Tang, J. Flexible Pressure Sensor with Ag Wrinkled Electrodes Based on PDMS Substrate. *Sensors* **2016**, *16*, 2131.
(42) Efros, A. L.; Shklovskii, B. I. Critical Behaviour of Conductivity and Dielectric Constant near the Metal-Non-Metal Transition Threshold. *Phys. Status Solidi B* **1976**, *76*, 475.
(43) Grannan, D. M.; Garland, J. C.; Tanner, D. B. Critical Behavior of the Dielectric Constant of a Random Composite near the Percolation Threshold. *Phys. Rev. Lett.* **1981**, *46*, 375.
(44) de Vries, D. V. W. M. Characterization of Polymeric Foams. Eindhoven Univ. Technol., 2009.
(45) Yoon, D. H.; Zhang, J.; Lee, B. I. Dielectric Constant and Mixing Model of BaTiO3 Composite Thick Films. *Mater. Res. Bull.* **2003**, *38*, 765.
(46) Qi, L.; Lee, B. I.; Chen, S.; Samuels, W. D.; Exarhos, G. J. High-Dielectric-Constant Silver-Epoxy Composites as Embedded Dielectrics. *Adv. Mater.* **2005**, *17*, 1777.
(47) Yoo, J. Y.; Seo, M. H.; Lee, J. S.; Choi, K. W.; Jo, M. S.; Yoon, J. B. Industrial Grade, Bending-Insensitive, Transparent Nanoforce Touch Sensor via Enhanced Percolation Effect in a Hierarchical Nanocomposite Film. *Adv. Funct. Mater.* **2018**, *28*, 1804721.
(48) Radu, M.; Bou-Said, B.; Cicone, T. Experimental Determination of Viscoelastic Properties of a Highly Compressible Porous Materials Imbibed with Water. *Mech. Ind.* **2015**, *16*, 606.
(49) Nguyen, S. T. Effect of Pore Shape on the Effective Behavior of Viscoelastic Porous Media. *Int. J. Solids Struct.* **2017**, *125*, 161.
(50) Kim, S.; Amjadi, M.; Lee, T.-I.; Jeong, Y.; Kwon, D.; Kim, M. S.; Kim, K.; Kim, T.-S.; Oh, Y. S.; Park, I. Wearable, Ultrawide-Range, and Bending-Insensitive Pressure Sensor Based on Carbon Nanotube Network-Coated Porous Elastomer Sponges for Human Interface and Healthcare Devices. *ACS Appl. Mater. Interfaces* **2019**, *11*, 23639.
(51) Wang, R.; Jia, W.; Mao, Z. H.; Sclabassi, R. J.; Sun, M. *Cuff-Free Blood Pressure Estimation Using Pulse Transit Time and Heart Rate*. In *International Conference on Signal Processing Proceedings*, ICSP: 2014.
(52) Luo, N.; Dai, W.; Li, C.; Zhou, Z.; Lu, L.; Poon, C. C. Y.; Chen, S. C.; Zhang, Y.; Zhao, N. Flexible Piezoresistive Sensor Patch Enabling Ultralow Power Cuffless Blood Pressure Measurement. *Adv. Funct. Mater.* **2016**, *26*, 1178.
(53) Oggioni, C.; Jakovljevic, D. G.; Klonizakis, M.; Ashor, A. W.; Ruddock, A.; Ranchordas, M.; Williams, E.; Siervo, M. Dietary Nitrate Does Not Modify Blood Pressure and Cardiac Output at Rest and during Exercise in Older Adults: A Randomised Cross-over Study. *Int. J. Food Sci. Nutr.* **2018**, *69*, 74.

NOTE ADDED AFTER ISSUE PUBLICATION

This paper was published on the Web on December 26, 2019, with Yong Suk Oh's name formatted incorrectly in the original version. The corrected version was reposted on April 3, 2020.

DOI: 10.1021/acsami.9b20097
ACS Appl. Mater. Interfaces 2020, 12, 1698−1706